

CtxMIM: Context-Enhanced Masked Image Modeling for Remote Sensing Image Understanding

Mingming Zhang, Qingjie Liu, and Yunhong Wang

State Key Laboratory of Virtual Reality Technology and Systems, Beihang University
Beijing, China

Abstract

Learning representations through self-supervision on unlabeled data has proven highly effective for understanding diverse images. However, remote sensing images often have complex and densely populated scenes with multiple land objects and no clear foreground objects. This intrinsic property generates high object density, resulting in false positive pairs or missing contextual information in self-supervised learning. To address these problems, we propose a context-enhanced masked image modeling method (CtxMIM), a simple yet efficient MIM-based self-supervised learning for remote sensing image understanding. CtxMIM formulates original image patches as a reconstructive template and employs a Siamese framework to operate on two sets of image patches. A context-enhanced generative branch is introduced to provide contextual information through context consistency constraints in the reconstruction. With the simple and elegant design, CtxMIM encourages the pre-training model to learn object-level or pixel-level features on a large-scale dataset without specific temporal or geographical constraints. Finally, extensive experiments show that features learned by CtxMIM outperform fully supervised and state-of-the-art self-supervised learning methods on various downstream tasks, including land cover classification, semantic segmentation, object detection, and instance segmentation. These results demonstrate that CtxMIM learns impressive remote sensing representations with high generalization and transferability. Code and data will be made public available.

1. Introduction

Remote sensing images have been widely used in many applications, including precision agriculture, disaster management, city planning, and environment monitoring. With a growing number of satellites collecting remote sensing images ceaselessly, abundant remote sensing images are easy to access, but annotations are technically challeng-



Figure 1. Object density differs between natural and remote sensing images. Natural images have apparent foreground objects in a relatively simple background, but remote sensing images contain multiple objects, especially no apparent foreground objects, in a vast complicated scene. Hence, extending MIM to remote sensing images will miss contextual information during reconstruction due to considerably high object density.

ing due to highly time-consuming and expertise knowledge than general benchmark datasets, *e.g.*, ImageNet [43]. Recently, self-supervised learning (SSL) has been increasingly emerging to pre-train models on large unlabeled data and demonstrate stronger performance than supervised learning on classification, segmentation, and detection. Therefore, the SSL paradigm has been receiving much attention from the remote sensing community and exploring to obtain an efficient pre-trained model on large-scale unlabeled data for remote sensing image understanding.

Existing advanced SSL methods [1, 3, 38, 39] primarily adopt contrastive learning [7–9] for self-supervised remote sensing representation learning. Indeed, contrastive learning-based approaches learn representations invariant to season, geographical location, illumination, and viewing angle by employing extensive data augmentation, which have preceded supervised learning-based methods. However, state-of-the-art contrastive methods typically require careful pre-training data organization in terms of temporal and geographical dimensions to prevent the pre-training collapse. Additionally, these methods generally obtain image-level features by comparing two augmented views.

Recently, SSL based on masked image modeling (MIM) has demonstrated potential performance in natural image representation learning [21, 56]. These MIM methods re-

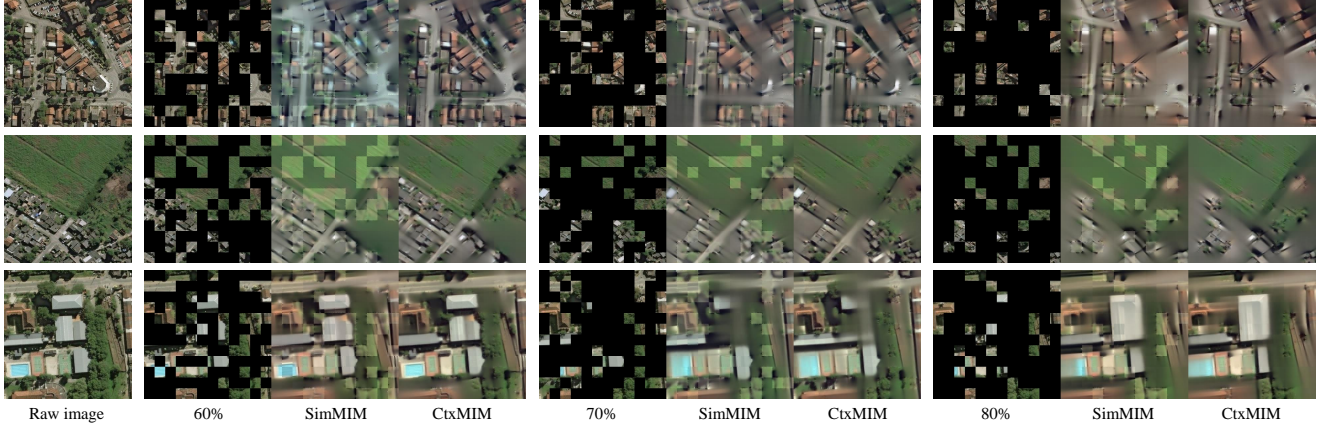


Figure 2. Reconstructive results on remote sensing images. The first column is the raw images. For the other three triples, we show the masked image with three masking ratios (left), SimMIM [56] reconstruction (middle), and our CtxMIM reconstruction (right). For SimMIM [56] and the proposed CtxMIM, we pre-train them on our collected remote sensing dataset. Although more and more land objects are masked as the ratio becomes larger, our CtxMIM can still reconstruct masked images better in terms of texture and content.

construct the masked patches by randomly masking an image with a high masking ratio (*e.g.*, 75% in MAE [21] and 80% in SimMIM [56]), which can learn good representations without extensive data augmentation. The pixel reconstruction idea of MIM is well-suited for remote sensing tasks since remote sensing analysis typically requires object-level or pixel-level features with fine-grained details rather than image-level features. However, applying MIM from natural images to remote sensing images still has limitations due to the considerably high object density in remote sensing images, as shown in Figure 1. Natural images have apparent foreground objects in a relatively simple background, *e.g.*, the cat, castle, and ambulance, which can be easily repaired by inferring the whole from some parts through rich contextual information in Figure 1. Since remote sensing images are captured by sensors mounted on satellites, they generally contain multiple objects in a vast complicated scene and typically have no apparent foreground objects, as illustrated in Figure 1. Unlike natural images, some small land objects may be entirely masked out by the randomly masking operation compared with natural images, as shown in Figure 1 and Table 7. Hence, MIM methods with a high masking ratio would hamper semantic extrapolating for remote sensing representation learning due to missing contextual information, as shown in Figure 2.

To address these issues, we propose a novel **C**ontext-enhanced **M**asked **I**mage **M**odeling method (CtxMIM) to learn representations with high-level semantic and fine-grained details for remote sensing image analysis. CtxMIM first adopts a pixel reconstructive pre-text task to capture local information from the masked image. Then, a context-enhanced generative branch formulates the original patches as the reconstructive template, encouraging the reconstructive

learning semantic extrapolating by providing meaningful contextual information. To train CtxMIM, a large-scale unlabeled dataset is collected, which contains over 1.28 million images without being carefully designed in terms of temporal and geographical dimensions.

We evaluate our approach on different tasks, including single-label and multi-label land cover classification, semantic segmentation, object detection, and instance segmentation. Following other remote sensing SSL methods, we use BigEarthNet [46], EuroSAT [23], xView [28], and SpaceNet [51] for comparison. Extensive experiments demonstrate that our method outperforms existing remote sensing SSL methods (up to +2.95%) and is more effective for remote sensing tasks than supervised learning on the common ImageNet [43] (up to +5.24%). In summary, our contributions are:

1. We propose a novel context-enhanced masked image modeling method (CtxMIM), a simple self-supervised learning framework to learn robust and transferable representations for efficient remote sensing image analysis.
2. CtxMIM is based on the analysis that remote sensing images have greatly higher object density than natural images. CtxMIM formulates the original image patches as the reconstructive template and introduces a context-enhanced generative branch to provide contextual information.
3. By pre-training on a large-scale unlabeled dataset, CtxMIM learns good representations to benefit image-level, object-level, and pixel-level downstream tasks. Moreover, we achieve state-of-the-art performance on single-label and multi-label land cover classification, semantic segmentation, object detection, and instance segmentation, demonstrating its transferability and superiority for remote sensing image analysis.

2. Related Work

2.1. Contrastive Learning

Contrastive learning methods [7–9, 16, 33, 41, 49, 58] can learn good representations by minimizing the distance between representations of two views augmented from one image (*i.e.*, positive pairs) and pushing the negative pairs from different images away. Recent contrastive learning methods [17, 27, 42, 59] have demonstrated their superiority in transferring to downstream tasks, even outperforming supervised learning. Although increasingly successful in many computer vision tasks, contrastive learning methods consider more image-level features, limiting the transferring performance in dense prediction cases requiring more local details.

2.2. Reconstructive Learning

Inspired by BERT [12] for masked language modeling, recent reconstructive learning methods [5, 21, 37, 55, 56] learn representations through solving the reconstructive pre-text task after employing a special [MASK] token to mask a portion of image patches randomly. MAE [21] first handles visible patches in the encoder, then encoded patches and mask tokens are processed in the decoder, which can significantly reduce the computation overhead of the encoder. SimMIM [56] only uses a lightweight prediction head to reconstruct raw pixel values of masked patches, facilitating good representation learning of the encoder. MixMAE [35] reconstructs two original images from the mixed image by replacing the original masked patches with visible patches of another image, improving pre-training efficiency and maintaining pretraining-finetuning consistency. With SOTA performance on many computer vision tasks, many related works have been studied, such as VideoMAE [50], MultiMAE [4], CIM [14], MSN [2], and SiamMAE [18]. However, these works have yet to be explored on large-scale remote sensing datasets.

2.3. Self-Supervised Learning in Remote Sensing

Recently, self-supervised learning has been broadly applied in remote sensing domains. For instance, [25, 26, 30, 45, 52] utilize contrastive learning to learn representations. SeCo [39] contrastively learns seasonal invariance by constructing a remote sensing dataset of different temporal information. [3, 31, 32] consider that geographical knowledge is the unique characteristic of remote sensing images, which can be used for contrastive learning. Inspired by classical material and texture methods, MATTER [1] leverages multi-temporal, spatially aligned remote sensing imagery over unchanged regions to learn representations invariance to illumination and viewing angle, finally achieving consistency of material and texture representations. Another attempt explores the masked image modeling paradigm for

remote sensing feature pre-training by repairing masked images, such as [47, 53]. SatMAE [11] based on Masked Autoencoder (MAE) leverages temporal and multi-spectral information for pre-training the network. Besides, more relevant works have been studied for special tasks, including change detection [6, 10, 54], land cover classification [24, 44, 57], and semantic segmentation [22, 29, 40, 48].

While many methods show improved performance on different downstream tasks, these methods are pre-trained on datasets by carefully organizing in terms of temporal and geographical dimensions, leading to poor generalization ability. Besides, the gap in object density information between natural and remote sensing images needs to be re-considered. Since remote sensing images contain multiple interesting objects rather than one obvious foreground object in natural images, existing remote sensing SSL methods remain challenging in the acquisition of positive pairs and reconstruction of masked image patches. This work designs self-supervised representation learning based on reconstruction with a context-enhanced generative branch, which can learn representations with rich semantic and fine-grained details.

3. Method

Figure 3 shows the pre-training pipeline of CtxMIM, and we will describe the main components in the following.

3.1. Overview

Our proposed CtxMIM is a novel context-enhanced self-supervised representation learning method based on reconstructive learning. Following the vision transformer, *e.g.*, ViT [13], CtxMIM first uniformly splits an input x into non-overlapping image patches x^p and then randomly mask x^p on patch-level to obtain a new input patches \hat{x}^p . Subsequently, CtxMIM takes as input \hat{x}^p to reconstruct the raw pixel values of the masked patches through the encoder-decoder architecture. Unlike natural images, the object density of remote sensing images is extremely uneven, resulting in missing contextual information when randomly masking image patches. To tackle this issue, we represent the original image patches as reconstructive templates rather than directly removing the masked patches, and introduce a context-enhanced generative branch to facilitate semantic reasoning by providing meaningful contextual information during the reconstruction. Moreover, the context-enhanced generative branch shares the encoder and the decoder with the reconstructive branch. Finally, our proposed CtxMIM is pre-trained on a large-scale unlabeled dataset and learns impressive representations, which is beneficial for various downstream tasks (*e.g.*, *image-level*, *object-level*, and *pixel-level*).

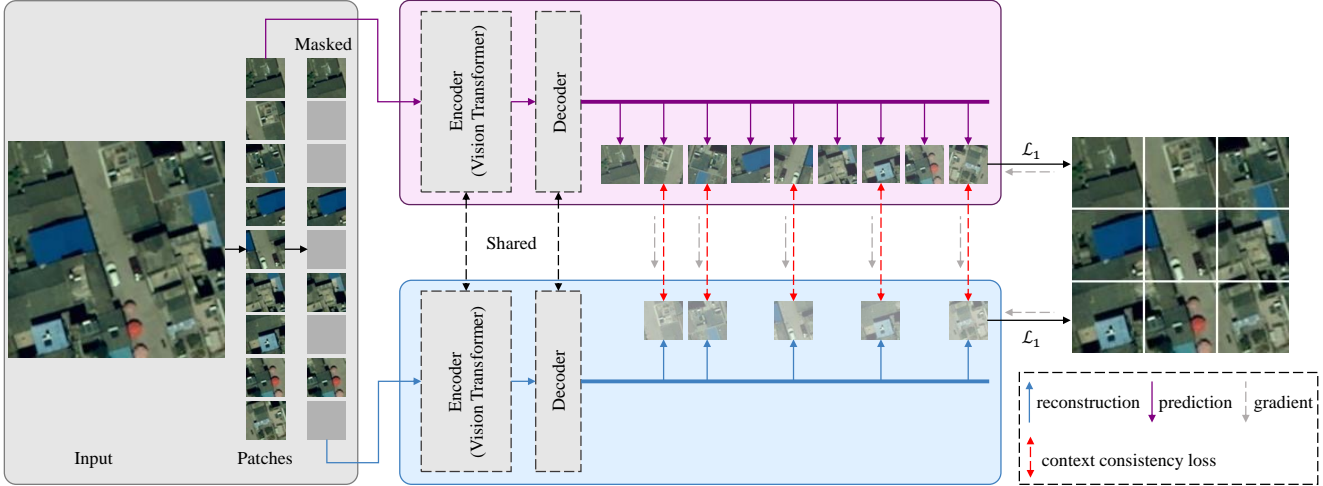


Figure 3. An illustration of CtxMIM, a simple yet efficient pre-training framework for remote sensing tasks. CtxMIM introduces a novel context-enhanced generative branch to provide contextual information by the context consistency constraint during the reconstruction, which formulates the original image patches as the reconstructive template. CtxMIM learns highly generalizable and transferable representations for various downstream tasks (e.g., image-level, object-level, and pixel-level).

3.2. Reconstruction of masked image patches

In the reconstruction stage, CtxMIM aims to learn local fine-grained features by restoring masked image patches. Given an input image $x \in \mathbb{R}^{C \times H \times W}$, CtxMIM firstly reshapes x to get image sequence patches $x^p \in \mathbb{R}^{N \times P^2 \times C}$, where H, W, C are the image height, width, and channel, respectively, P is the size of each image patch (i.e., the height and width), and $N = (H/P) \cdot (W/P)$ is the number of image patches. Then, a patch-wise masking operation randomly masks some image patches, and a patch embedding operation encodes each image patch to get the new sequence input \hat{x}^p . Subsequently, an encoder f_θ takes the sequence input \hat{x}^p to extract latent representations h^p , which are used in downstream tasks after pre-training. Finally, a decoder g_θ is used to reconstruct pixel values of masked patches \hat{y}^p on the latent representations. In our paper, we take Swin Transformer [36] as the feature encoder f_{swin} and a lightweight prediction head as the decoder g_{mlp} to output raw pixel values of the masked patches by following SimMIM [56], which can be formulated as:

$$\hat{y}^p = g_{mlp}(f_{swin}(\hat{x}^p) \odot \mathbb{I}_{\mathcal{M}}(\hat{x}_i^p)) \quad (1)$$

where $\mathbb{I}_{\mathcal{M}}(\cdot)$ is an indicator function that is 1 when each image patch \hat{x}_i^p is masked, 0 otherwise. \odot is an element-wise product operation.

3.3. Context-enhanced generative branch

Compared with natural images that captured in daily scenes and objects are mostly with large size, remote sensing images typically cover multiple land objects with a large-scale and complex scene, which have no clear foreground

objects. Therefore, some small land covers could be entirely masked, resulting in missing critical contextual information during the reconstruction. To tackle this issue, CtxMIM introduces a context-enhanced generative branch to provide contextual information. As illustrated in Figure 3, the context-enhanced generative branch inputs the image patches x^p to extract latent representations h^p with rich contextual information by the shared encoder f_θ . Then, the latent representations h^p are fed to the same decoder g_θ to predict the raw pixels y^p .

3.4. Training objective

CtxMIM first realizes a reconstructive learning objective by minimizing the distance between raw pixel values X and the reconstructive values Y_{Re} :

$$L_{Re} = \frac{\|Y_{Re} - X\|}{N} \quad (2)$$

where N is the number of masked pixels. $\|\cdot\|$ is a distance function for calculating similarity between Y_{Re} and X (e.g., L_1 or L_2 loss).

For the context-enhanced generative branch, CtxMIM adopts the Equation 2 to learn contextual information by calculating the predicted loss L_{Pr} between the predicted pixel values Y_{Pr} and raw pixel values X . Then, a context consistency loss L_{Cc} maximizes the similarity between Y_{Re} and the corresponding portion of Y_{Pr} , which is defined as:

$$L_{Cc} = \text{Dist}(Y_{Re} - Y_{Pr}) \quad (3)$$

where $\text{Dist}(\cdot)$ is a similarity function to guide CtxMIM learning good contextual information.

Finally, the joint training objective is:

$$L = L_{Re} + L_{Pr} + L_{Cc} \quad (4)$$

CtxMIM learns representations with rich semantic and local information by pre-training in a multi-task learning manner.

4. Experiments

This section describes datasets and experiment settings for pre-training and transfer learning. We evaluate our model on five downstream tasks and compare its performance with SOTA methods quantitatively and qualitatively. Finally, we conduct extensive ablation studies to verify the effectiveness of the proposed pre-training framework. Additionally, more details of datasets and experiment settings for pre-training and transfer learning are described in the appendix.

4.1. Pre-training

Dataset. Existing remote sensing SSL methods carefully construct pre-training datasets in temporal and geographic dimensions, limiting the scalability of the pre-training model and the transferability of learned features to some extent. Without careful organization for extensive data augmentations, we collect a large-scale unlabeled remote sensing dataset captured from the WorldView-3 using Google Earth Engine [15]. This pre-training dataset covers most regions of Asia, including cities, villages, rivers, mountains, woodlands, and other terrain. Some examples of the pre-training dataset are shown in Figure 4. In our experiments, we crop images into 192×192 pixels and get 1,287,248 image patches to train the proposed CtxMIM.

Implementation Details. The proposed CtxMIM adopts Swin-B as the encoder and is implemented by the PyTorch framework with 8 NVIDIA Tesla V100 GPUs. We use AdamW optimizer with hyper-parameters $\beta_1 = 0.9$, $\beta_2 = 0.999$, and $\epsilon = 1 \times 10^{-8}$, and the learning rate is set to 1×10^{-5} . The training lasts 200 epochs with a batch size of 112 per GPU.

4.2. Transfer Learning Settings

In downstream experiments, we select single/multi-label land cover classification, semantic segmentation, object detection, and instance segmentation, covering image-level, object-level, and pixel-level remote sensing tasks. To comprehensively confirm the performance of our method, we compare CtxMIM with supervised learning and SOTA self-supervised learning methods. Finally, extensive experiments show that CtxMIM has strong performance on downstream tasks.

Sup. We employ two general backbones (ResNet-50 [19] and Swin Transformer [36]) initialized with ImageNet pre-training and random weights for supervised learning com-



Figure 4. The pre-training dataset in our work, which consists of 1.28M images comparable to ImageNet. The large-scale, comprehensive dataset contains rich topography and terrain without careful organization and will be available for further research.

parison. In Tabs. 1 to 6, R50_Random, R50_IN, and Swin-B_IN denote that different backbones (ResNet-50 and Swin-B) initialized with random initialization and ImageNet pre-training, respectively.

Self-Sup. For self-supervised learning comparison, we evaluate our approach with contrastive methods (SeCo [39], Ayush et al. [3], and CACo [38]) and a reconstructive method SatMAE [11]. Following the comparison SSL methods, we use EuroSAT [23], BigEarthNet [46], SpaceNet (Rio and Las Vegas) [51], and xView [28] to evaluate different tasks.

4.3. Land Cover Classification on EuroSAT

Implementation Details. EuroSAT [23] is a single-label land cover classification dataset composing of Sentinel-2 satellite images. EuroSAT contains 10 classes and has 27,000 labeled images with a size of 64×64 . Following SeCo [39] and SatMAE [11], we adopt the official train/val splits on the EuroSAT.

For the single-label land cover classification task, we initialize a Swin-B backbone with our pre-trained weight and fine-tune a linear classifier head on top with ground truth labels in a supervised manner. We use an AdamW optimizer, a batch size of 32, a learning rate of 1×10^{-3} , and finally report the top-1 accuracy for performance comparison.

Quantitative Results. Table 1 shows the top-1 accuracy of the different methods using fully supervised and self-supervised learning. We can see that CtxMIM outperforms the ImageNet supervised Swin-B backbone by +2.92%, illustrating that SSL on a large-scale remote sensing dataset improves performance for remote sensing downstream tasks. Compared with contrastive and reconstructive methods, CtxMIM respectively achieves +2.31% and +2.95% higher top-1 accuracy, demonstrating that our approach learns robust and good transferable remote sensing representations for the land cover classification task.

Table 1. Top-1 accuracy on the EuroSAT for single-label land cover classification. CtxMIM gets the best performance.

	Method	Top-1 Acc. \uparrow
Sup.	R50_Random	55.32
	R50_IN	89.08
	Swin-B_IN	95.77
Self-Sup.	SeCo [39]	95.43
	Ayush et al. [3]	96.38
	CACo [38]	95.90
	SatMAE [11]	95.74
	CtxMIM (ours)	98.69

Table 2. Mean average precision (mAP) on the BigEarthNet for multi-label land cover classification.

	Method	mAP \uparrow
Sup.	R50_Random	78.98
	R50_IN	86.74
	Swin-B_IN	83.62
Self-Sup.	SeCo [39]	87.81
	Ayush et al. [3]	82.36
	CACo [38]	78.58
	SatMAE [11]	84.73
	CtxMIM (ours)	86.88

4.4. Land Cover Classification on BigEarthNet

Implementation Details. BigEarthNet [46] is a large-scale Sentinel-2 dataset comprising 590,326 images across 10 European countries. Each image is annotated with multiple labels from 19 land cover classes, so we report the mean average precision (mAP) of all categories to measure the performance of different methods. Following SeCo [39], we omit patches covered by seasonal snow, clouds, or cloud shadows and use the same train/val splits for this experiment.

We fine-tune a classifier head on top of our pre-trained Swin-B backbone. We use an AdamW optimizer, a batch size of 96, a learning rate of 0.0001, and a weight decay of 0.005. Besides, we use 10% of the train set to evaluate the label efficient transfer learning by following SatMAE [11].

Quantitative Results. In Table 2, we observe that CtxMIM improves the model of the Swin-B backbone initialized with the ImageNet supervised pre-training by +3.26% higher, proving that the domain gap exists between natural and remote sensing images. Table 3 reports the performance of different methods on 10% of BigEarthNet’s labeled data. We find that CtxMIM outperforms ImageNet supervised pre-training with the Swin-B backbone by +3.9% and achieves +0.54% higher than SatMAE [11]. Extensive experiments show that CtxMIM is more label-efficient than other comparison methods.

Table 3. Label-efficient transfer learning on 10% of the BigEarth-Net. Our method is more label-efficient than other comparison methods.

	Method	mAP \uparrow
Sup.	R50_Random	69.49
	R50_IN	80.04
	Swin-B_IN	78.77
Self-Sup.	SeCo [39]	82.62
	Ayush et al. [3]	80.20
	CACo [38]	71.18
	SatMAE [11]	82.13
	CtxMIM (ours)	82.67

Table 4. Mean intersection over union (mIoU) on the SpaceNet (Rio) semantic segmentation task. Our method consistently improves supervised and self-supervised learning by large margins.

	Method	mIoU \uparrow
Sup.	R50_Random	75.57
	R50_IN	75.61
	Swin-B_IN	74.23
Self-Sup.	SeCo [39]	77.09
	Ayush et al. [3]	78.51
	CACo [38]	77.94
	SatMAE [11]	78.07
	CtxMIM (ours)	79.47

4.5. Semantic Segmentation

Implementation Details. We use SpaceNet (Rio) dataset [51] for the semantic segmentation task. This dataset contains 6,940 satellite images with binary building masks.

Following SatMAE [11], we fine-tune a PSANet [60] with the pre-trained Swin-B backbone by CtxMIM. We use an AdamW optimizer with a batch size of 8, a learning rate of 6×10^{-5} , and a weight decay of 0.01. We report mean intersection over union (mIoU) to compare CtxMIM with comparison methods.

Quantitative Results. Table 4 presents mIoU values on the SpaceNet (Rio) of different methods. The results show that our method achieves more considerable performance gains by +5.24% for supervised learning from the ImageNet pre-trained weight with the Swin-B backbone and +1.4% compared with SatMAE [11]. Consistent experimental results demonstrate the effectiveness of our method for the semantic segmentation task. Figure 5 shows visible results for the SpaceNet semantic segmentation task by Sup. and Self-Sup. methods, proving that CtxMIM can learn more robust features for dense remote sensing understanding.

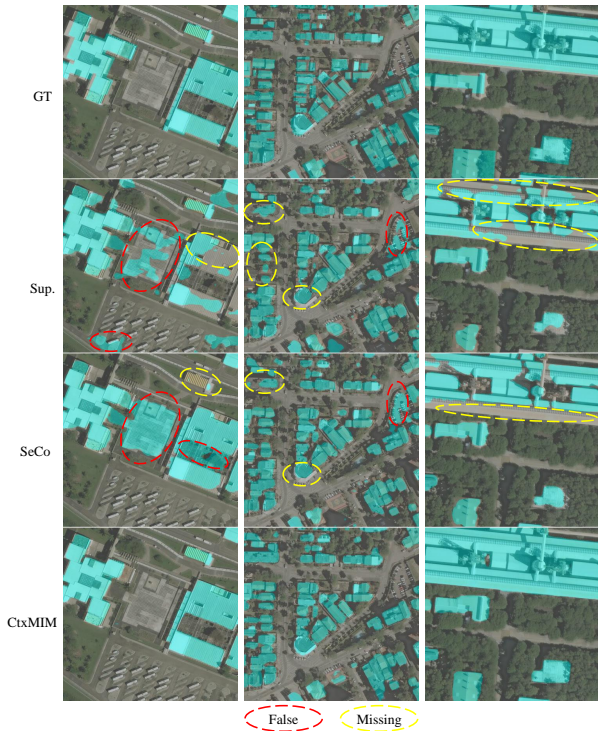


Figure 5. Qualitative results of PSANet on the SpaceNet (Rio) for semantic segmentation. CtxMIM can segment arbitrary objects of different sizes and shapes. Zoom in for a clearer view.

4.6. Object Detection

Implementation Details. Following Ayush et al. [3], we use the xView dataset [28] to verify the object detection performance. The xView dataset contains 846 satellite images with a size of about 3000×2000 pixels at 0.3m ground sample distance. This dataset has 60 categories with bounding box annotation and is split into 416×416 pixels. Then, we fine-tune a RetinaNet [34] with an AdamW optimizer, a batch size of 4, a learning rate of 1×10^{-5} , and a weight decay of 0.05. We use the indicator AP_{50} to compare CtxMIM with Sup. and Self-Sup. methods on this task.

Quantitative Results. Table 5 lists results from comprehensive experiments on the xView dataset compared with supervised and self-supervised learning methods. CtxMIM achieves 18.80% AP_{50} , improving the self-supervised learning method [3] by +1.1%. The extraordinary performance demonstrates that CtxMIM learns impressive representations for the object detection task.

4.7. Instance Segmentation

Implementation Details. The SpaceNet (LasVegas) dataset [51] is used for instance segmentation, consisting of 3851 images across Las Vegas. The size of images is 650×650 pixels with a spatial resolution of 30 cm/pixel.

Table 5. AP_{50} on the xView object detection task. Our method improves the SOTA method by +1.1%, demonstrating the transferability of learned features by our method for object detection.

	Method	$AP_{50} \uparrow$
Sup.	R50_Random	14.4
	R50_IN	14.4
	Swin-B_IN	16.3
Self-Sup.	SeCo [39]	14.7
	Ayush et al. [3]	17.7
	CACo [38]	17.2
	CtxMIM (ours)	18.8

Table 6. AP^m , AP_{50}^m , and AP_{75}^m on the SpaceNet (Las Vegas) instance segmentation task. CtxMIM outperforms comparison methods (+1.4% and +1.0% for Sup. and Self-Sup., respectively).

	Method	AP^m	AP_{50}^m	AP_{75}^m
Sup.	R50_Random	58.2	86.2	70.1
	R50_IN	60.2	86.9	72.7
	Swin-B_IN	59.1	86.8	70.7
Self-Sup.	SeCo [39]	58.4	86.5	70.5
	Ayush et al. [3]	58.9	86.6	70.8
	CACo [38]	59.5	86.7	71.5
	SatMAE [11]	52.4	83.7	61.1
	CtxMIM (ours)	60.5	87.8	72.9

In our experiment, this dataset is randomly divided into train/test/validation subsets with a ratio of 8:1:1. We fine-tune MaskRCNN [20] with the pre-trained Swin-B backbone from our CtxMIM on the SpaceNet (LasVegas), using an AdamW optimizer, a learning rate of 0.0001, a batch size of 8. Finally, we report the AP^m , AP_{50}^m , and AP_{75}^m under different intersection over union (IoU) thresholds in the segmentation level.

Quantitative Results. As shown in Table 6, our approach learns transferable representations outperforming all the comparison methods. Especially, CtxMIM improves the ImageNet supervised pre-training with the Swin-B backbone by +1.4% AP^m , +1% AP_{50}^m , and +2.2% AP_{75}^m , respectively. Moreover, CtxMIM achieves +8.1% AP^m , +4.1% AP_{50}^m , and +11.8% AP_{75}^m higher compared with SatMAE [11]. The impressive results illustrate that CtxMIM learns good representations with high-level semantic and fine-grained details. Figure 6 shows the visualization comparison of Mask RCNN on the SpaceNet (Las Vegas) from different pre-training methods, comprehensively illustrating the transferability of representations. From qualitative results, CtxMIM generates high-quality instance segmentation of different sizes and shapes, demonstrating that CtxMIM learns more transferable features for remote sensing image analysis.

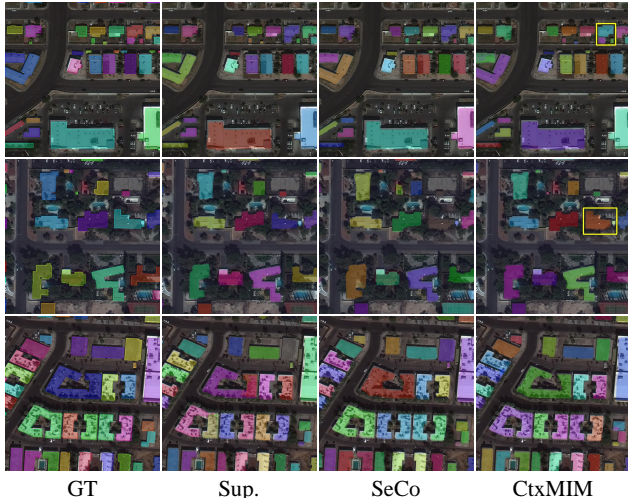


Figure 6. Qualitative results of Mask RCNN on the SpaceNet (Las Vegas) initialized with different pre-training weights to show feature transferability. CtxMIM generates high-quality masks of different sizes and shapes, demonstrating that CtxMIM learns more transferable features for remote sensing image analysis. Zoom in for a clearer view.

Table 7. Ablation study. LcC, SS, OD, and IS denote land cover classification, semantic segmentation, object detection, and instance segmentation, respectively. ‘- C-E’ removes the context-enhanced generative branch from CtxMIM.

Method	LcC (Acc.)	SS (mIoU)	OD (AP_{50})	IS (AP^m)
CtxMIM (ours)	98.69	79.47	18.80	60.50
- C-E	96.90	76.91	16.30	59.10

4.8. Ablation Study

We conduct ablation studies to verify the effectiveness of the designed context-enhanced generative branch on four typical remote sensing tasks, respectively. In Table 7, ablation results have confirmed that the context-enhanced generative branch can significantly improve the performance (up to +2.56%), illustrating its superiority.

5. Discussion

In this section, we further analyze our method in terms of model structure and performance, share our observations, and discuss limitations and future work about SSL in remote sensing.

Model scalability. SSL methods in remote sensing employ contrastive learning to pre-train foundation models and have demonstrated higher performance on different remote sensing tasks. For extensive data augmentations, these methods consider intrinsic characteristics of remote sensing im-

ages to obtain contrastive pairs, like SeCo [39], CACo [38], and SatMAE [11] leveraging the temporal information, and Ayush et al. [3] leveraging geo-location information. However, the well-designed data structure is a double-edged sword that limits the capabilities of foundation models to some extent. Besides, remote sensing image pairs are sensitive to significant changes in the temporal span, such as major urban development [38], natural disasters, and the external environment. Hence, the natural advantage of abundant remote sensing images captured by sensors daily should be reconsidered, making the foundation model easily extended to a larger scale in further research.

Exploring more effective SSL paradigm. Unlike natural images, remote sensing images generally cover a large and complex scene, leading to a considerably high object density. Due to the gap in object density information, advanced SSL methods in remote sensing still suffer from **3M** problem: (1) **Mismatched** positive pairs augmented from one remote sensing image; (2) **Missing** contextual information caused by random masking strategies; (3) **Mechanism** in pre-training dataset collection. We rethink: *is SSL paradigm effective for remote sensing representation learning?* We explore this answer from the characteristics of remote sensing data and tasks. Since most remote sensing tasks are dense predictions at object-level or pixel-level, contrastive method learning representations from two augmented views is less optimal for remote sensing analysis. This work leverages the original image patches masked in MIM to learn good representations and has illustrated its performance on various tasks.

Limitations and future work. Although CtxMIM is a simple yet powerful MIM method for remote sensing pre-training, we argue that collaborative learning by combining contrastive and reconstructive learning can yield robust representations for remote sensing analysis. In future work, we will explore a new paradigm of collaborative learning, design a more efficient mask strategy, and employ patch pairs of masked and original to jointly embed contrastive learning into reconstructive learning. With the simple pipeline and the solid performance, we hope this work will inspire other works, not just in the remote sensing community but also in the industry and medical image analysis community.

6. Conclusion

This paper presents CtxMIM, a simple yet efficient MIM method for remote sensing representation learning. CtxMIM is based on the insight that the high object density in remote sensing images significantly impedes semantic reasoning for reconstructive learning due to missing contextual information. Therefore, CtxMIM formulates the original patches as reconstructive templates and introduces a context-enhanced generative branch to provide contextual information using the context consistency constraint. Moreover, we train CtxMIM by collecting a large-scale unlabeled

remote sensing dataset with 1.28 million images covering rich topography and terrain. Comprehensive experiments on land cover classification, semantic segmentation, object detection, and instance segmentation demonstrate that CtxMIM learns impressive representations with high generalization and transferable ability, significantly outperforming fully supervised and self-supervised learning methods.

References

- [1] Peri Akiva, Matthew Purri, and Matthew Leotta. Self-supervised material and texture representation learning for remote sensing tasks. In *IEEE Conference on Computer Vision and Pattern Recognition (CVPR)*, pages 8203–8215, 2022. [1](#), [3](#)
- [2] Mahmoud Assran, Mathilde Caron, Ishan Misra, Piotr Bojanowski, Florian Bordes, Pascal Vincent, Armand Joulin, Mike Rabbat, and Nicolas Ballas. Masked siamese networks for label-efficient learning. In *European Conference on Computer Vision (ECCV)*, pages 456–473, 2022. [3](#)
- [3] Kumar Ayush, Burak Uzkent, Chenlin Meng, Kumar Tanmay, Marshall Burke, David Lobell, and Stefano Ermon. Geography-aware self-supervised learning. In *IEEE International Conference on Computer Vision (ICCV)*, pages 10181–10190, 2021. [1](#), [3](#), [5](#), [6](#), [7](#), [8](#)
- [4] Roman Bachmann, David Mizrahi, Andrei Atanov, and Amir Zamir. Multimaec: Multi-modal multi-task masked autoencoders. In *European Conference on Computer Vision (ECCV)*, pages 348–367, 2022. [3](#)
- [5] Hangbo Bao, Li Dong, Songhao Piao, and Furu Wei. Beit: Bert pre-training of image transformers. *arXiv preprint arXiv:2106.08254*, 2021. [3](#)
- [6] Hao Chen, Wenyuan Li, Song Chen, and Zhenwei Shi. Semantic-aware dense representation learning for remote sensing image change detection. *IEEE Transactions on Geoscience and Remote Sensing*, 60:1–18, 2022. [3](#)
- [7] Ting Chen, Simon Kornblith, Mohammad Norouzi, and Geoffrey Hinton. A simple framework for contrastive learning of visual representations. In *International Conference on Machine Learning (ICML)*, pages 1597–1607, 2020. [1](#), [3](#)
- [8] Xinlei Chen and Kaiming He. Exploring simple siamese representation learning. In *IEEE Conference on Computer Vision and Pattern Recognition (CVPR)*, pages 15750–15758, 2021.
- [9] Xinlei Chen, Haoqi Fan, Ross Girshick, and Kaiming He. Improved baselines with momentum contrastive learning. *arXiv preprint arXiv:2003.04297*, 2020. [1](#), [3](#)
- [10] Yuxing Chen and Lorenzo Bruzzone. Self-supervised change detection in multiview remote sensing images. *IEEE Transactions on Geoscience and Remote Sensing*, 60:1–12, 2022. [3](#)
- [11] Yezhen Cong, Samar Khanna, Chenlin Meng, Patrick Liu, Erik Rozi, Yutong He, Marshall Burke, David Lobell, and Stefano Ermon. Satmae: Pre-training transformers for temporal and multi-spectral satellite imagery. *Advances in Neural Information Processing Systems (NeurIPS)*, 35:197–211, 2022. [3](#), [5](#), [6](#), [7](#), [8](#)
- [12] Jacob Devlin, Ming-Wei Chang, Kenton Lee, and Kristina Toutanova. Bert: Pre-training of deep bidirectional transformers for language understanding. *arXiv preprint arXiv:1810.04805*, 2018. [3](#)
- [13] Alexey Dosovitskiy, Lucas Beyer, Alexander Kolesnikov, Dirk Weissenborn, Xiaohua Zhai, Thomas Unterthiner, Mostafa Dehghani, Matthias Minderer, Georg Heigold, Sylvain Gelly, Jakob Uszkoreit, and Neil Houlsby. An image is worth 16x16 words: Transformers for image recognition at scale. *International Conference on Learning Representations (ICLR)*, 2021. [3](#)
- [14] Yuxin Fang, Li Dong, Hangbo Bao, Xinggang Wang, and Furu Wei. Corrupted image modeling for self-supervised visual pre-training. *arXiv preprint arXiv:2202.03382*, 2022. [3](#)
- [15] Noel Gorelick, Matt Hancher, Mike Dixon, Simon Ilyushchenko, David Thau, and Rebecca Moore. Google earth engine: Planetary-scale geospatial analysis for everyone. *Remote sensing of Environment*, 202:18–27, 2017. [5](#)
- [16] Jean-Bastien Grill, Florian Strub, Florent Alché, Corentin Tallec, Pierre Richemond, Elena Buchatskaya, Carl Doersch, Bernardo Avila Pires, Zhaohan Guo, Mohammad Gheshlaghi Azar, et al. Bootstrap your own latent-a new approach to self-supervised learning. *Advances in Neural Information Processing Systems (NeurIPS)*, 33:21271–21284, 2020. [3](#)
- [17] Tianyu Guo, Hong Liu, Zhan Chen, Mengyuan Liu, Tao Wang, and Runwei Ding. Contrastive learning from extremely augmented skeleton sequences for self-supervised action recognition. In *AAAI Conference on Artificial Intelligence*, pages 762–770, 2022. [3](#)
- [18] Agrim Gupta, Jiajun Wu, Jia Deng, and Li Fei-Fei. Siamese masked autoencoders. *arXiv preprint arXiv:2305.14344*, 2023. [3](#)
- [19] Kaiming He, Xiangyu Zhang, Shaoqing Ren, and Jian Sun. Deep residual learning for image recognition. In *IEEE Conference on Computer Vision and Pattern Recognition (CVPR)*, pages 770–778, 2016. [5](#)
- [20] Kaiming He, Georgia Gkioxari, Piotr Dollár, and Ross Girshick. Mask r-cnn. In *IEEE International Conference on Computer Vision (ICCV)*, pages 2961–2969, 2017. [7](#)
- [21] Kaiming He, Xinlei Chen, Saining Xie, Yanghao Li, Piotr Dollár, and Ross Girshick. Masked autoencoders are scalable vision learners. In *IEEE Conference on Computer Vision and Pattern Recognition (CVPR)*, pages 16000–16009, 2022. [1](#), [2](#), [3](#)
- [22] Shuyi He, Qingyong Li, Yang Liu, and Wen Wang. Semantic segmentation of remote sensing images with self-supervised semantic-aware inpainting. *IEEE Geoscience and Remote Sensing Letters*, 19:1–5, 2022. [3](#)
- [23] Patrick Helber, Benjamin Bischke, Andreas Dengel, and Damian Borth. Eurosat: A novel dataset and deep learning benchmark for land use and land cover classification. *IEEE Journal of Selected Topics in Applied Earth Observations and Remote Sensing*, 12(7):2217–2226, 2019. [2](#), [5](#)
- [24] Haozhe Huang, Zhongfeng Mou, Yunying Li, Qiujuan Li, Jie Chen, and Haifeng Li. Spatial-temporal invariant contrastive learning for remote sensing scene classification. *IEEE Geoscience and Remote Sensing Letters*, 19:1–5, 2022. [3](#)

- [25] Heechul Jung, Yoonju Oh, Seongho Jeong, Chaehyeon Lee, and Taegyun Jeon. Contrastive self-supervised learning with smoothed representation for remote sensing. *IEEE Geoscience and Remote Sensing Letters*, 19:1–5, 2021. 3
- [26] Jian Kang, Ruben Fernandez-Beltran, Puhong Duan, Sicong Liu, and Antonio J Plaza. Deep unsupervised embedding for remotely sensed images based on spatially augmented momentum contrast. *IEEE Transactions on Geoscience and Remote Sensing*, 59(3):2598–2610, 2020. 3
- [27] Daeha Kim and Byung Cheol Song. Contrastive adversarial learning for person independent facial emotion recognition. In *AAAI Conference on Artificial Intelligence*, pages 5948–5956, 2021. 3
- [28] Darius Lam, Richard Kuzma, Kevin McGee, Samuel Doolley, Michael Laielli, Matthew Klaric, Yaroslav Bulatov, and Brendan McCord. xviv: Objects in context in overhead imagery. *arXiv preprint arXiv:1802.07856*, 2018. 2, 5, 7
- [29] Haifeng Li, Yi Li, Guo Zhang, Ruoyun Liu, Haozhe Huang, Qing Zhu, and Chao Tao. Global and local contrastive self-supervised learning for semantic segmentation of hr remote sensing images. *IEEE Transactions on Geoscience and Remote Sensing*, 60:1–14, 2022. 3
- [30] Wenyuan Li, Hao Chen, and Zhenwei Shi. Semantic segmentation of remote sensing images with self-supervised multi-task representation learning. *IEEE Journal of Selected Topics in Applied Earth Observations and Remote Sensing*, 14:6438–6450, 2021. 3
- [31] Wenyuan Li, Keyan Chen, Hao Chen, and Zhenwei Shi. Geographical knowledge-driven representation learning for remote sensing images. *IEEE Transactions on Geoscience and Remote Sensing*, 60:1–16, 2021. 3
- [32] Wenyuan Li, Keyan Chen, and Zhenwei Shi. Geographical supervision correction for remote sensing representation learning. *IEEE Transactions on Geoscience and Remote Sensing*, 60:1–20, 2022. 3
- [33] Yunfan Li, Peng Hu, Zitao Liu, Dezhong Peng, Joey Tianyi Zhou, and Xi Peng. Contrastive clustering. In *AAAI conference on Artificial Intelligence*, pages 8547–8555, 2021. 3
- [34] Tsung-Yi Lin, Priya Goyal, Ross Girshick, Kaiming He, and Piotr Dollár. Focal loss for dense object detection. In *IEEE International Conference on Computer Vision (ICCV)*, pages 2980–2988, 2017. 7
- [35] Jihao Liu, Xin Huang, Jinliang Zheng, Yu Liu, and Hongsheng Li. Mixmae: Mixed and masked autoencoder for efficient pretraining of hierarchical vision transformers. In *IEEE Conference on Computer Vision and Pattern Recognition (CVPR)*, pages 6252–6261, 2023. 3
- [36] Ze Liu, Yutong Lin, Yue Cao, Han Hu, Yixuan Wei, Zheng Zhang, Stephen Lin, and Baining Guo. Swin transformer: Hierarchical vision transformer using shifted windows. In *IEEE International Conference on Computer Vision (ICCV)*, pages 10012–10022, 2021. 4, 5
- [37] Zhengqi Liu, Jie Gui, and Hao Luo. Good helper is around you: Attention-driven masked image modeling. In *AAAI Conference on Artificial Intelligence*, pages 1799–1807, 2023. 3
- [38] Utkarsh Mall, Bharath Hariharan, and Kavita Bala. Change-aware sampling and contrastive learning for satellite images. In *IEEE Conference on Computer Vision and Pattern Recognition (CVPR)*, pages 5261–5270, 2023. 1, 5, 6, 7, 8
- [39] Oscar Manas, Alexandre Lacoste, Xavier Giró-i Nieto, David Vazquez, and Pau Rodriguez. Seasonal contrast: Unsupervised pre-training from uncurated remote sensing data. In *IEEE International Conference on Computer Vision (ICCV)*, pages 9414–9423, 2021. 1, 3, 5, 6, 7, 8
- [40] Dilxat Muhtar, Xueliang Zhang, and Pengfeng Xiao. Index your position: A novel self-supervised learning method for remote sensing images semantic segmentation. *IEEE Transactions on Geoscience and Remote Sensing*, 60:1–11, 2022. 3
- [41] Aaron van den Oord, Yazhe Li, and Oriol Vinyals. Representation learning with contrastive predictive coding. *arXiv preprint arXiv:1807.03748*, 2018. 3
- [42] Tal Reiss and Yedid Hoshen. Mean-shifted contrastive loss for anomaly detection. In *AAAI Conference on Artificial Intelligence*, pages 2155–2162, 2023. 3
- [43] Olga Russakovsky, Jia Deng, Hao Su, Jonathan Krause, Sanjeev Satheesh, Sean Ma, Zhiheng Huang, Andrej Karpathy, Aditya Khosla, Michael Bernstein, et al. Imagenet large scale visual recognition challenge. *International Journal of Computer Vision (IJCV)*, 115:211–252, 2015. 1, 2
- [44] Linus Scheibenreif, Joëlle Hanna, Michael Mommert, and Damian Borth. Self-supervised vision transformers for land-cover segmentation and classification. In *IEEE Conference on Computer Vision and Pattern Recognition (CVPR)*, pages 1422–1431, 2022. 3
- [45] Vladan Stojnic and Vladimir Risojevic. Self-supervised learning of remote sensing scene representations using contrastive multiview coding. In *IEEE Conference on Computer Vision and Pattern Recognition (CVPR)*, pages 1182–1191, 2021. 3
- [46] Gencer Sumbul, Marcela Charfuelan, Begüm Demir, and Volker Markl. Bigearthnet: A large-scale benchmark archive for remote sensing image understanding. In *IEEE International Geoscience and Remote Sensing Symposium (IGARSS)*, pages 5901–5904, 2019. 2, 5, 6
- [47] Xian Sun, Peijin Wang, Wanxuan Lu, Zicong Zhu, Xiaonan Lu, Qibin He, Junxi Li, Xuee Rong, Zhujun Yang, Hao Chang, et al. Ringmo: A remote sensing foundation model with masked image modeling. *IEEE Transactions on Geoscience and Remote Sensing*, 61:1–22, 2023. 3
- [48] Maofeng Tang, Konstantinos Georgiou, Hairong Qi, Cody Champion, and Marc Bosch. Semantic segmentation in aerial imagery using multi-level contrastive learning with local consistency. In *IEEE Winter Conference on Applications of Computer Vision*, pages 3798–3807, 2023. 3
- [49] Yonglong Tian, Dilip Krishnan, and Phillip Isola. Contrastive multiview coding. In *European Conference on Computer Vision (ECCV)*, pages 776–794, 2020. 3
- [50] Zhan Tong, Yibing Song, Jue Wang, and Limin Wang. Videomae: Masked autoencoders are data-efficient learners for self-supervised video pre-training. *Advances in Neural Information Processing Systems (NeurIPS)*, 35:10078–10093, 2022. 3

- [51] Adam Van Etten, Dave Lindenbaum, and Todd M Bacastow. Spacenet: A remote sensing dataset and challenge series. *arXiv preprint arXiv:1807.01232*, 2018. 2, 5, 6, 7
- [52] Stefano Vincenzi, Angelo Porrello, Pietro Buzzega, Marco Cipriano, Pietro Fronte, Roberto Cucu, Carla Ippoliti, Annamaria Conte, and Simone Calderara. The color out of space: learning self-supervised representations for earth observation imagery. In *International Conference on Pattern Recognition (ICPR)*, pages 3034–3041, 2021. 3
- [53] Di Wang, Qiming Zhang, Yufei Xu, Jing Zhang, Bo Du, Dacheng Tao, and Liangpei Zhang. Advancing plain vision transformer toward remote sensing foundation model. *IEEE Transactions on Geoscience and Remote Sensing*, 61:1–15, 2022. 3
- [54] Jue Wang, Yanfei Zhong, and Liangpei Zhang. Change detection based on supervised contrastive learning for high-resolution remote sensing imagery. *IEEE Transactions on Geoscience and Remote Sensing*, 61:1–16, 2023. 3
- [55] Chen Wei, Haoqi Fan, Saining Xie, Chao-Yuan Wu, Alan Yuille, and Christoph Feichtenhofer. Masked feature prediction for self-supervised visual pre-training. In *IEEE Conference on Computer Vision and Pattern Recognition (CVPR)*, pages 14668–14678, 2022. 3
- [56] Zhenda Xie, Zheng Zhang, Yue Cao, Yutong Lin, Jianmin Bao, Zhuliang Yao, Qi Dai, and Han Hu. Simmim: A simple framework for masked image modeling. In *IEEE Conference on Computer Vision and Pattern Recognition (CVPR)*, pages 9653–9663, 2022. 1, 2, 3, 4
- [57] Zhixiang Xue, Xuchu Yu, Anzhu Yu, Bing Liu, Pengqiang Zhang, and Shentong Wu. Self-supervised feature learning for multimodal remote sensing image land cover classification. *IEEE Transactions on Geoscience and Remote Sensing*, 60:1–15, 2022. 3
- [58] Jure Zbontar, Li Jing, Ishan Misra, Yann LeCun, and Stéphane Deny. Barlow twins: Self-supervised learning via redundancy reduction. In *International Conference on Machine Learning (ICML)*, pages 12310–12320, 2021. 3
- [59] Xinyun Zhang, Binwu Zhu, Xufeng Yao, Qi Sun, Ruiyu Li, and Bei Yu. Context-based contrastive learning for scene text recognition. In *AAAI Conference on Artificial Intelligence*, pages 3353–3361, 2022. 3
- [60] Hengshuang Zhao, Yi Zhang, Shu Liu, Jianping Shi, Chen Change Loy, Dahua Lin, and Jiaya Jia. Psanet: Point-wise spatial attention network for scene parsing. In *ECCV*, pages 267–283, 2018. 6